Arabian Journal for Science and Engineering (2018) 43:3065–3081
https://doi.org/10.1007/s13369-018-3109-2

RESEARCH ARTICLE - ELECTRICAL ENGINEERING

Power Quality and Stability Improvement of Hybrid Energy System Under Weak Grid Environment

Rahul Sharma[1] · **Sathans Suhag**[1]

Received: 8 March 2017 / Accepted: 4 February 2018 / Published online: 13 February 2018

Abstract
This paper proposes the control scheme using super-capacitor (SC) in hybrid energy system (HES) under the weak grid condition. Photovoltaic-based HES connected to weak grid is considered as the system under study. The control scheme is designed for power quality improvement, reduction of ripple content in DC link voltage and to improve the stability margin of HES by utilizing SC. The proposed control scheme is very effective in reducing the ripples in the current, improving the dynamic response and damping out the oscillations under transient conditions. Unlike with conventional control, the stability of the DC link voltage controller under the proposed control scheme is independent of weak grid conditions. Drawbacks of the conventional control schemes, due to the coupling terms and variable grid impedance in weak grid condition, are analyzed and illustrated mathematically. Design and stability analysis of the proposed control scheme is described and compared with the conventional control scheme. HES is modeled and simulated in MATLAB Simulink to verify the enhanced performance of the proposed control scheme over conventional control scheme in terms of improvement in DC link voltage profile, reduction in ripple content in power and better dynamic response of HES connected to weak grid.

Keywords Hybrid energy system · Photovoltaic · Super-capacitor · Stability · Weak grid

1 Introduction

In today's world, with sharp rise in consumption of power and at the same time the increased environmental concerns coupled with the limited fossil fuel, the power generation from non-conventional energy sources is increasing exponentially. This has been made possible due to the developments of modern power electronics components in the recent past decades. Therefore, today, the renewable energy sources offer the best solution of power generation to meet economical constraints, sustainability, reliability as well as environmental constraints [1]. But renewable energy sources have their own limitations [2]. Different renewable energy-based system configurations like standalone system, grid-connected system, microgrid based system have been reported in the literature to ensure continuous, efficient and quality power supply. The recent literature suggests that hybrid renewable energy system offers the best possible solution in the recent scenario. However, there are many stability and control challenges that need to be addressed in order to make a hybrid energy system more reliable, stable and cost-effective along with improved power quality under different conditions [3]. But, stability and power quality are the main concerns in a weak grid environment, where low-voltage, high-impedance network is offered by weak grid [4]. In the grid, the condition where short-circuit ratio (SCR) is less than three and grid impedance is significant and has to be taken into account in order to draw a valid conclusion, is known as weak grid condition. To enhance the power quality, much focus is needed to mitigate the voltage fluctuations, ripples in power, to bring about improvement in transient behavior, dynamic response and stability of the system. The above issues have to be addressed to provide improved quality and cost-effective power to the consumers.

In the recent literature, control strategies have been proposed to increase stability margin and improve power quality under weak grid condition. Authors in [5] proposed grid-connected and islanding mode control to suppress the voltage fluctuation under transition periods from grid to islanding mode or vice versa, but it compromises transient performance and quality in a steady state, where the ripples are

✉ Rahul Sharma
rahulsharma.knit2006@gmail.com

[1] Electrical Engineering, National Institute of Technology, Kurukshetra 136119, India

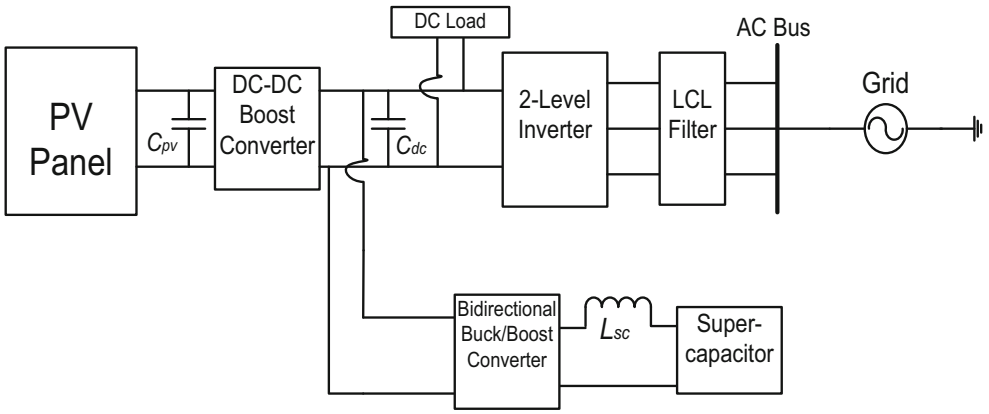

Fig. 1 Schematic diagram of hybrid energy system

present in the power waveform due to the coupling components. In [6], improved control strategy has been proposed for weak grid-connected inverter using adaptive control to improve transient performance and suppress the harmonics, but system stability is affected under microgrid environment, where local constant and dynamic ac/dc loads are also connected to the point of common coupling (PCC). Authors in [7] proposed multivariable droop control under microgrid conditions to enhance the stability and current sharing, but variable impedance of the line is not considered in decoupling terms, which reduces system stability margin and introduces ripples in output waveforms. A novel frequency and voltage control method is proposed in [8] for islanded microgrid, based on multi-energy storages with virtual impedance control, to increase stability margin, but estimation of virtual impedance is not accurate; thus, this mismatch of virtual impedance under sudden change in operating conditions may result in instability. In [9], an improved control method is proposed for multiple power converters in hybrid ac/dc microgrid to achieve power sharing and better circulating current, but, it compromised the stability and power quality of the system. In [10], the control strategy results in enhanced quality of power to sensitive loads connected to the AC bus in microgrid environment, but, proper decoupling method is absent in control scheme and also stability analysis is not discussed for the proposed control, where large impedance of line cannot be ignored. Virtual negative resistor-based control for inverters is proposed in [11] for low-voltage microgrid to improve margin of the system stability and power sharing under drift in line impedance parameters, but, in microgrid environment, having variable line impedance, proposed control is unable to handle instability and poor transient behavior due to frequent change in load or source input or temperature of the conductors, reflected as impedance drift. Virtual impedance droop control schemes are proposed in [12–14] to improve active/reactive power coupling and stability margin, but, they have not taken grid impedance coupling terms in inner voltage control into account and as a result the stability analysis is not accurate. In [15], control scheme for ac/dc microgrid is proposed for power sharing between AC and DC grids as well as stability improvements, but, DC link voltage regulation is poor and AC side voltage controller stability margin reduces under variable impedance of AC bus. As all the cited literature is based on conventional control schemes with minor modifications, this paper proposes novel control scheme to address the aforesaid problems of HES connected to weak grid in different operating conditions. No similar control scheme has yet been reported in the literature.

Proposed control scheme is implemented on HES consisting of PV panel as renewable energy source, SC as energy storage device and power electronics converters as power conditioning devices, as in Fig. 1. In conventional control scheme, for efficient utilization, the hybrid energy systems are working on both grid as well as islanded mode, but energy storage devices in HES are used to maintain DC link voltage constant under islanding mode only, whereas in grid-connected mode, energy storage devices are just connected to the system in standby. Therefore, the proposed control scheme is different from the conventional control scheme because of the following:

- Unlike conventional way, in this paper, SC, as an energy storage device, is used to participate in the control of the inverter under grid-connected condition as well.
- The proposed control scheme does not use PLL to determine synchronization angle, instead adopts different proposed method for the purpose and non-use of PLL improves the bandwidth of the control scheme.
- The fast charging/discharging rate of SC is utilized in the proposed control to make the response of the current controller faster as compared to conventional control, where it is sluggish.

The proposed control scheme is designed to utilize the energy storage device, the SC, in both grid-connected as well as islanded modes to increase the bandwidth of stability, improve the slow response of the system, provide better transient response and smoothening of the power oscillations. Proposed control scheme is designed to utilize the property of fast charging/discharging rate of SC, as discussed in [16,17].

In this paper, the control scheme is proposed, by using a SC, for gird connected mode to:

(i) increase the stability margin under variable and high grid impedance condition.
(ii) regulate DC link voltage and improve dynamic as well as the steady-state response of the HES.
(iii) achieve better transient response and damp out the power oscillations.
(iv) improve power quality by reducing steady-state ripples due to lower-order harmonics.

This paper is divided into the following four sections besides Introduction section: Sect. 2 covers the analysis of the conventional control scheme and design of the proposed control scheme for HES in weak grid condition. Section 3 includes the design and stability analysis of conventional and proposed control schemes of HES under different grid impedance conditions. Section 4 demonstrates the simulation results of the HES connected to weak grid in different operating conditions and brings out a comparison of the results along with the conventional control scheme. Lastly, Sect. 5 concludes the findings of this study by highlighting the effectiveness of the proposed control scheme.

2 System Description and Control Scheme

Figure 2 shows the configuration of the inverter connected to the grid through an inductance–capacitance–inductance (LCL) filter with a SC connected to the DC link of the inverter. Buck–boost DC–DC converter is utilized to connect SC, which consists of inductance L_{sc} and bidirectional switches SW_3/SW_4 where, i_{sc} is SC current, d_{sc} is duty cycle and v_{sc} is the SC voltage. The LCL filter consists of inductances L_1, L_2 and capacitance C_f, as configured in Fig. 2, whereas the detailed designing of LCL filter has been reported in the literature [18,19] and can be referred. The grid is connected at PCC, where U_{sabc} is the grid ideal voltage, Z_g is grid impedance, i_g is injected current into the grid, i_c is capacitor current, i_{inv} is inverter side current, and U_{gabc} is the grid voltage at PCC. Park's transformation [20] is used to transform stationary reference frame (abc) into the synchronous reference frame ($d-q$). P^* is the power generated by the PV system, P_g is the power injected into the grid, K_p is the droop gain of the synchronizing control loop, ω is the actual frequency of the system, ω^* (2*50*3.14) is the desired frequency of the system, and θ is the synchronizing angle.

2.1 Conventional Control Structure for HES Connected to Weak Grid

Conventional control of grid-connected LCL inverter [21] to control DC link voltage and reactive power is shown in Fig. 3. $U*_{dc}$ is reference DC link voltage, where reference d-axis grid current $i*_{gd}$ is the output of the DC link voltage controller, while $i*_{gq}$ is the reference q-axis grid current chosen as zero to regulate reactive power for unity power factor, where $U*_d$ and $U*_q$ are the outputs of the grid current control loops and taken as the voltage references for inverter switching and ω is the grid frequency.

Now, the equation of voltages can be written as:

$$U_d = L\frac{di_{gd}}{dt} + U_{gd} - \omega L i_{gq} \tag{1}$$

$$U_q = L\frac{di_{gq}}{dt} + U_{gq} + \omega L i_{gd} \tag{2}$$

where, $L = L_1 + L_2$

With the help of feed-forward decoupled control, output of the current controller ΔU, the voltage error, is added to the actual voltages to get the reference voltages as

$$U_d^* = \Delta U_d + U_{gd} - \omega L i_{gq} \tag{3}$$

$$U_q^* = \Delta U_q + U_{gq} + \omega L i_{gd} \tag{4}$$

But, in weak grid condition, the conventional control scheme is not appropriate to provide quality power output to be injected into the grid due to the reasons which are analyzed as follows:

(1) Under transient response, changes in load or input power are directly reflected into reference currents as

$$i_{gd}^* = \Delta i_{gd} + i_{gd} \tag{5}$$

$$i_{gq}^* = \Delta i_{gq} + i_{gq} \tag{6}$$

where Δi_{gd} and Δi_{gq} are the DC values of changes that get added up and directly reflected into the reference currents under transient condition. But, these transient changes do not get directly reflected into the feed-forward decoupled control components $-\omega L i_{gq}$ and $\omega L i_{gd}$; therefore, as a result, the dynamic response of the grid current control loop is slow.

(2) Voltage controller stability is the main concern in a weak grid condition, where the grid impedance is unknown variable over a wide range and depends on operating

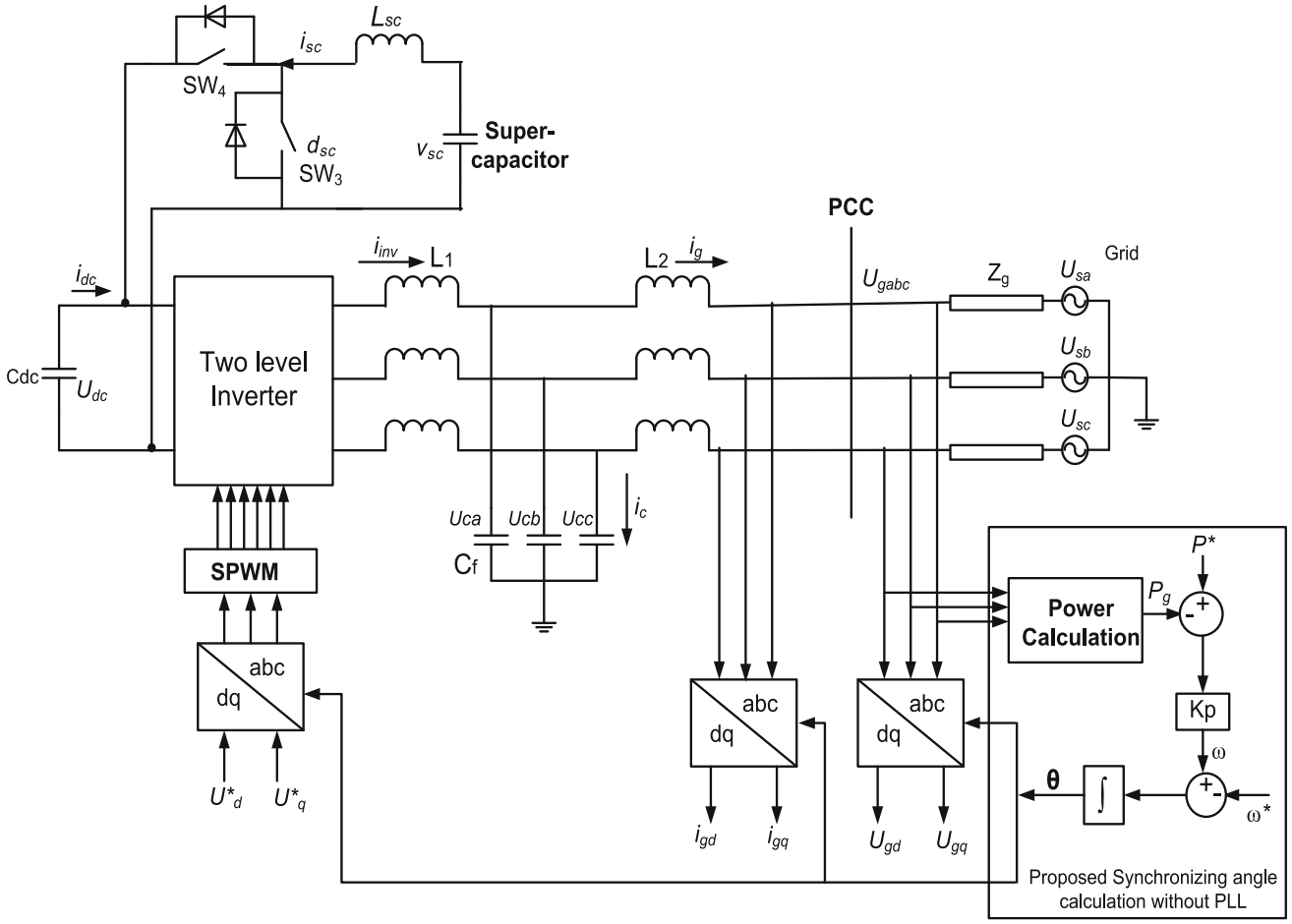

Fig. 2 Structure of inverter connected to weak grid with LCL filter and super-capacitor

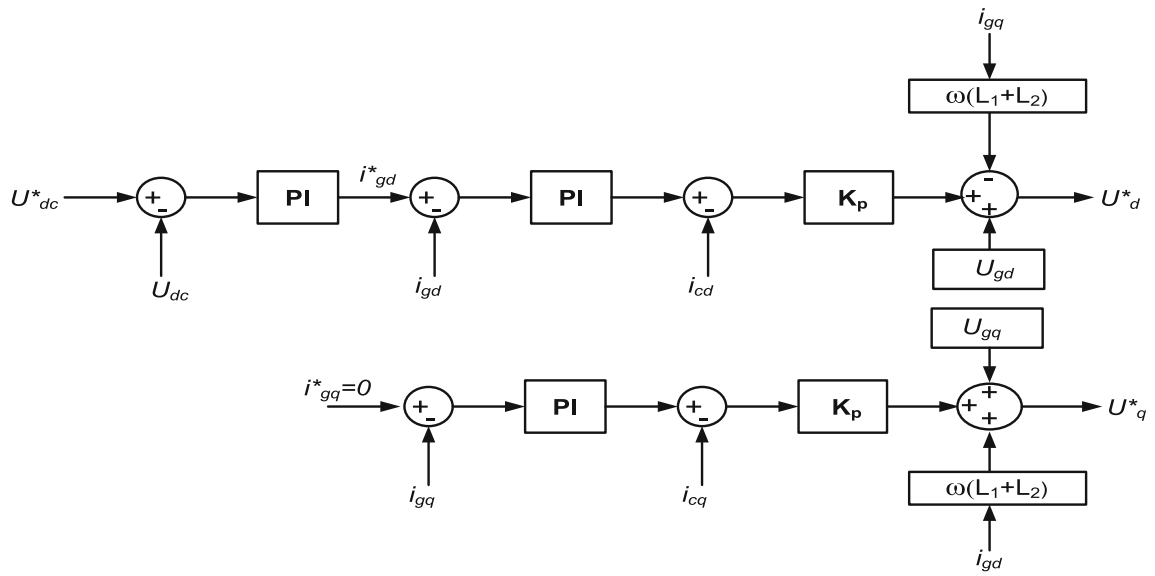

Fig. 3 Conventional control scheme for grid-connected inverter

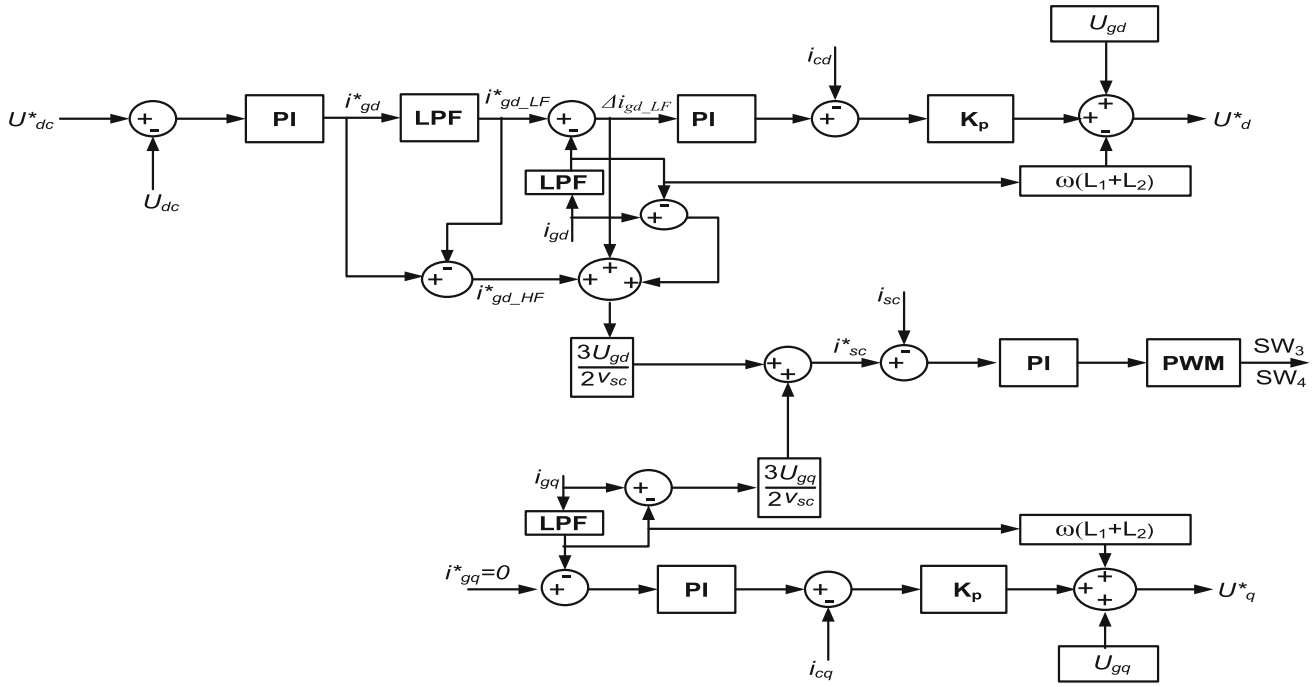

Fig. 4 Proposed control scheme of HES for the grid-connected mode

conditions. Voltage control loop is the outer loop, and grid current control loop is the inner loop. Bandwidth of voltage control loop is maintained less than grid current control loop because voltage control loop is slower than current control loop. Therefore, in weak grid case, where grid impedance is considered, the feed-forward decoupled control must compensate for $-\omega L i_{\mathrm{gq}} - \omega L_{\mathrm{g}} i_{\mathrm{gq}}$ and $\omega L i_{\mathrm{gd}} + \omega L_{\mathrm{g}} i_{\mathrm{gd}}$. Therefore, Eqs. (3) and (4) can be written as,

$$U_{\mathrm{d}}^{*} = \Delta U_{\mathrm{d}} + U_{\mathrm{gd}} - \omega L i_{\mathrm{gq}} - \omega L_{\mathrm{g}} i_{\mathrm{gq}} \tag{7}$$

$$U_{\mathrm{q}}^{*} = \Delta U_{\mathrm{q}} + U_{\mathrm{gq}} + \omega L i_{\mathrm{gd}} + \omega L_{\mathrm{g}} i_{\mathrm{gd}} \tag{8}$$

But, L_{g} is unknown grid inductance and therefore cannot be compensated using feed-forward decoupled control. As a result, coupling components of grid inductance reduce the current control loop stability margin. Therefore, in the conventional approach, under large value of grid inductance L_{g}, feed-forward decoupled control seriously compromises the robustness of the current control loop in the weak grid condition. The stability of the outer voltage control loop is adversely affected because proportional integral (PI) controller of the voltage control loop is tuned based on inner grid current control loop. In most cases, under large grid inductance variations, voltage controller becomes unstable.

(3) Steady-state ripples also remain present in the grid current as nonlinear loads inject lower-order harmonics at steady state, which the conventional control scheme is not able to suppress. Therefore, grid current at steady state can be written as:

$$i_{\mathrm{gd}} = i_{\mathrm{gd}}^{*} + \hat{i}_{\mathrm{gd}} \tag{9}$$

$$i_{\mathrm{gq}} = i_{\mathrm{gq}}^{*} + \hat{i}_{\mathrm{gq}} \tag{10}$$

where $\hat{i}_{\mathrm{gd}}$ and $\hat{i}_{\mathrm{gq}}$ are the steady-state ripple currents. These steady-state ripples reduce the waveform quality of grid current. Furthermore, ripple current components affect the coupling terms. Now, reference voltages at steady state can be written as:

$$U_{\mathrm{d}}^{*} = \Delta U_{\mathrm{d}} + U_{\mathrm{gd}} - \omega L i_{\mathrm{gq}} - \omega L \hat{i}_{\mathrm{gq}} \tag{11}$$

$$U_{\mathrm{q}}^{*} = \Delta U_{\mathrm{q}} + U_{\mathrm{gq}} - \omega L i_{\mathrm{gd}} - \omega L \hat{i}_{\mathrm{gd}} \tag{12}$$

As the reference voltages contain the terms $-\omega L \hat{i}_{\mathrm{gq}}$ and $\omega L \hat{i}_{\mathrm{gd}}$ as per (11) and (12), this will interact and worsen the waveform quality of the grid current and power further.

2.2 Proposed Control Structure for HES Connected to Weak Grid

Figure 4 shows the proposed control scheme of hybrid energy system for grid-connected mode. This scheme involves an outer voltage control loop, inner grid current control loop

(for d and q-axis) and inner SC current control loop. The SC is having fast charging/discharging rate; hence, the dynamic response of the SC current control loop is faster than that of grid current control loop [22]. Therefore, SC current control loop is utilized to compensate for transients and steady-state ripples in power. To utilize SC fast dynamic characteristics, SC current control loop is designed and develops relations between all control loops by the mathematical analysis as follows:

The output of the outer voltage control loop is reference grid current, $i*_{gd}$, which is separated by the low-pass filter (LPF) into two components as average current component (DC value), $i*_{gd\_LF}$, and high-frequency current component, $i*_{gd\_HF}$. Therefore, reference grid current can be written as:

$$i^*_{gd} = i^*_{gd\_LF} + i^*_{gd\_HF} \tag{13}$$

$$i^*_{gq} = i^*_{gq\_LF} + i^*_{gq\_HF} \tag{14}$$

Under transient conditions, reference grid current contains DC value $i*_{gd\_LF}$ and high-frequency current component $i*_{gd\_HF}$. Now, reference power, $p*_g$, is needed to be injected into the grid for power balancing and DC link voltage regulation, whereas p_g is the actual power being injected into the grid and can be written as:

$$p_g = \frac{3}{2}(U_{gd} i_{gd} + U_{gq} i_{gq}) \tag{15}$$

whereas,

$$p^*_g = \frac{3}{2}(U_{gd} i^*_{gd} + U_{gq} i^*_{gq}) \tag{16}$$

But, $i^*_{gq} = 0$, therefore, $p^*_g = \frac{3}{2} U_{gd} i^*_{gd}$ and from (13) can be written as,

$$p^*_g = \frac{3}{2}(U_{gd} i^*_{gd\_LF} + U_{gd} i^*_{gd\_HF}) \tag{17}$$

Equation (17) can be rewritten with the help of (5) as

$$p^*_g = \frac{3}{2}\left(U_{gd} i_{gd\_LF} + U_{gd}\Delta i_{gd\_LF} + U_{gd} i^*_{gd\_HF}\right) \tag{18}$$

Now, as per (18), the reference power comprises three components to be injected into the grid, which are $\frac{3}{2} U_{gd} i_{gd\_LF}$, the actual power component without steady-state ripples, $\frac{3}{2} U_{gd}\Delta i_{gd\_LF}$, the DC value of change in power and $\frac{3}{2} U_{gd}$ $i^*_{gd\_HF}$, the high-frequency component responsible for ripples under transient conditions. Besides the actual power component, the additional power required for compensation is

$$p_{un\_comp} = \frac{3}{2} U_{gd}\Delta i_{gd\_LF} + \frac{3}{2} U_{gd} i^*_{gd\_HF} \tag{19}$$

where $\frac{3}{2} U_{gd} i^*_{gd\_HF}$ is the high-frequency component which does not exist in a steady-state condition, but it must be damped out as early as possible to improve transient response. The grid current control loop cannot damp out the high-frequency component; however, SC current control loop is able to compensate for high-frequency component by its inherent characteristics of fast charging/discharging. Therefore, this component is compensated by SC. Similarly, $\frac{3}{2} U_{gd}\Delta i_{gd\_LF}$, the DC value of change in power component is compensated by grid current control loop, but it takes a long time due to the slow dynamic response of the grid current control loop. Therefore, initially this component is also compensated by SC current control loop to improve the dynamic response of the voltage control loop.

Under steady-state condition, ripples are present in grid current due to lower-frequency harmonics. Therefore, the grid current can be written as:

$$i_{gd} = i^*_{gd\_LF} + \hat{i}_{gd} \tag{20}$$

$$i_{gq} = i^*_{gq\_LF} + \hat{i}_{gq} \tag{21}$$

Ripple currents can be extracted by LPF under steady state. Ripples are high-frequency components, whereas steady-state grid currents are DC values. Therefore,

$$p_{ripple} = \frac{3}{2}\left(U_{gd}\,\hat{i}_{gd} + U_{gq}\,\hat{i}_{gq}\right) \tag{22}$$

Steady-state ripple currents inject ripples in power, which get reflected in the form of ripples in DC link voltage. These ripples can be damped out by compensating ripple power p_{ripple} with the help of a SC current control loop.

Now, the total compensating power p_{comp}, as needed to compensate for transients and ripples, can be written as:

$$p_{comp} = \frac{3}{2} U_{gd}\left(\Delta i_{gd\_LF} + i^*_{gd\_HF} + \hat{i}_{gd}\right) + \frac{3}{2} U_{gq}\,\hat{i}_{gq} \tag{23}$$

Therefore, SC reference current i^*_{sc} can be obtained as:

$$i^*_{sc} = \frac{3}{2}\frac{U_{gd}}{v_{sc}}\left(\Delta i_{gd\_LF} + i^*_{gd\_HF} + \hat{i}_{gd}\right) + \frac{3}{2}\frac{U_{gq}}{v_{sc}}\,\hat{i}_{gq} \tag{24}$$

With the help of (24), the proposed control scheme is shown in Fig. 4, where output of SC current control loop generates the switching signal for bidirectional buck–boost converter switches SW_3 and SW_4 while inner grid current control loops generate signal to control inverter switches.

In the proposed control scheme under weak grid condition, the voltage control loop is not affected by wide variations in grid inductance, which provides robustness and stability to the control scheme. Therefore, the proposed control scheme

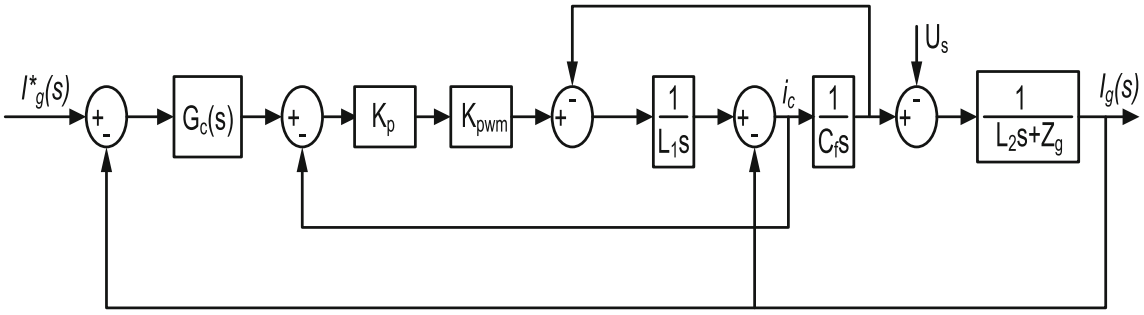

Fig. 5 Mathematical model of weak grid-connected inverter current control

provides better stability margin, fast dynamic response and improved waveform quality under weak grid conditions as compared to conventional one.

3 Design and Stability Analysis

3.1 Conventional Control Scheme

Stability of the conventional control scheme is analyzed by considering voltage control loop bandwidth as maintained less as compared to inner current control loop because the voltage PI controller is tuned based on inner current control loop. Figure 5 shows the transfer function model, adapted from [24], of inverter current control connected to weak grid, which consists of inner loop—a proportional regulator—and outer loop—a PI regulator. This model is used to analyze the stability, the detailed description of which can be referred from [24]. Switching frequency f_s of inverter is taken as 10 kHz. Where, $G_c(s)$ is gain of outer loop PI regulator, K_p is the gain of proportional regulator, and K_{pwm} is the gain of inverter.

From Fig. 5, the closed-loop transfer function is

$$G_{cl\_i}(s) = \frac{I_g(s)}{I_g^*(s)} = \frac{G_c(s)K_pK_{pwm}}{L_1L_2C_fs^3 + K_1s^2 + K_2s + K_3} \tag{25}$$

where, $K_1 = (L_2K_pK_{pwm} + L_1Z_g)C_f$, $K_2 = L_1 + L_2 + Z_gC_fK_pK_{pwm}$ and $K_3 = G_c(s)K_pK_{pwm} + Z_g$

The open-loop transfer function of voltage control loop can be derived as per Fig. 6, where $G_v(s)$ is the gain of PI voltage controller and $G_{cl\_i}(s)$ is the grid current closed-loop control gain.

Now, voltage control loop has three controller gains: $G_v(s)$, $G_c(s)$ and K_p where, $G_v(s)$ and $G_c(s)$ can be written as:

$$G_v(s) = K_{p\_v} + \frac{K_{i\_v}}{s} \tag{26}$$

$$G_c(s) = K_{p\_c} + \frac{K_{i\_c}}{s} \tag{27}$$

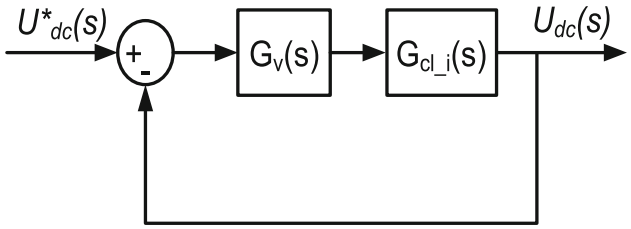

Fig. 6 Block diagram of voltage controller with conventional control scheme

Therefore, open-loop transfer function $G_{ol\_v}(s)$ of voltage control loop can be written as

$$G_{ol\_v}(s) = G_v(s)G_{cl\_i}(s) \tag{28}$$

The controllers are designed to achieve high bandwidth and good stability margin by using diagram-aided method [23]. K_{pwm} is assumed as unity. Now, phase margin (P.M.) and gain margin (G.M.) are 103° and 15 dB, respectively, obtained in MATLAB from the open-loop Bode plot of $G_{ol\_v}(s)$. The cutoff frequency is around 2 kHz (approximately $f_s/5$).

Now, the impact of the grid impedance on the stability of the voltage control loop at conventional scheme is analyzed. The impact of the grid resistance is negligible in the control scheme [24]. Assuming $r_g = 0$, the effect of L_g is studied. The open-loop Bode plots are shown in Fig. 7 with different values of grid inductance L_g for voltage control loop. When $L_g = 2$ mH, phase and gain margins are 103° and 8.19 dB, respectively, which still provides good stability margin but the value of gain margin decreases as compared to initial value. Similarly, at $L_g = 3$ mH, the voltage control loop stability margins: P.M. and G.M. decrease sharply to 5.56° and 1.81 dB, respectively. Further, the voltage control loop becomes unstable when $L_g = 3.5, 4$ mH or more where both phase and gain margins become negative, as shown in Fig. 7.

Under the weak gird condition, stability analysis shows that the conventional control scheme does not provide good stability margins and robustness of voltage control loop and not only this, even system instability arises under large values of grid inductance.

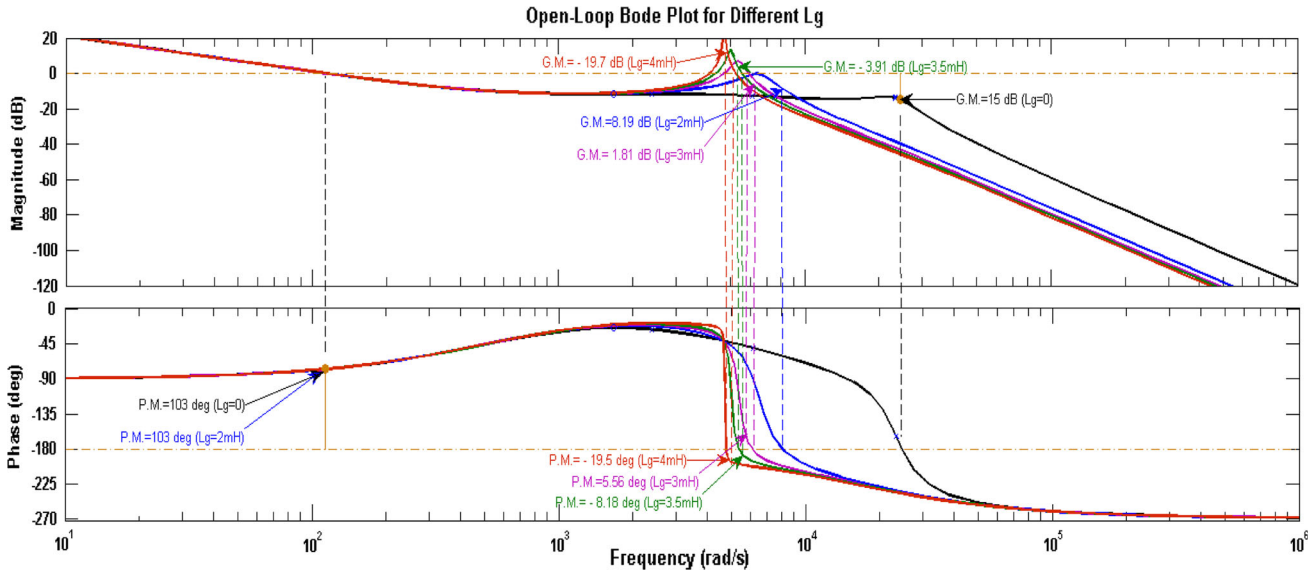

Fig. 7 Bode plots of the voltage control loop

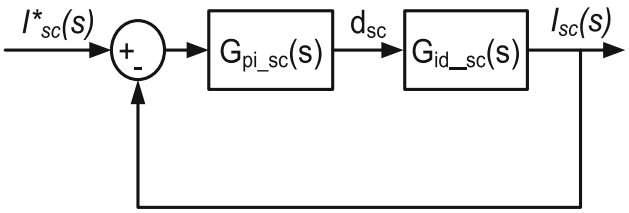

Fig. 8 Block diagram of SC current controller

3.2 Proposed Control Scheme

In the proposed control scheme, voltage and grid current control loops are designed and their stability analyzed separately because both are independent of each other. SC current control loop is faster than grid current control loop; therefore, the voltage control loop is tuned based on SC current control loop. Figure 8 shows the SC current control loop where $G_{\mathrm{pi\_sc}}(s)$ is the gain of PI regulator and $G_{\mathrm{id\_sc}}(s)$ is the gain of bidirectional dc/dc buck–boost converter [25].

Therefore, $G_{\mathrm{pi\_sc}}(s)$ and $G_{\mathrm{id\_sc}}(s)$ can be written as:

$$G_{\mathrm{pi\_sc}}(s) = K_{\mathrm{p\_sc}} + \frac{K_{\mathrm{i\_sc}}}{s} \tag{29}$$

$$G_{\mathrm{id\_sc}}(s) = \frac{U_{\mathrm{dc}}C_{\mathrm{dc}}s + 2i_{\mathrm{dc}}}{L_{\mathrm{sc}}C_{\mathrm{dc}}s^2 + (U_{\mathrm{dc}}/i_{\mathrm{dc}})L_{\mathrm{sc}}s + (1-d_{\mathrm{sc}})^2} \tag{30}$$

Now, closed-loop transfer function of SC current control $G_{\mathrm{cl\_sc}}(s)$ can be written as,

$$G_{\mathrm{cl\_sc}}(s) = \frac{G_{\mathrm{pi\_sc}}(s)G_{\mathrm{id\_sc}}(s)}{1 + G_{\mathrm{pi\_sc}}(s)G_{\mathrm{id\_sc}}(s)} \tag{31}$$

Figure 9 shows the voltage control loop based on SC current control loop, which consists of $G_{\mathrm{v}}(s)$ as PI regulator gain, $G_{\mathrm{cl\_sc}}(s)$ as transfer function of closed-loop SC current control loop and $G_{\mathrm{v\_dc}}(s)$ as transfer function of SC inductor current to DC link voltage.

Therefore, $G_{\mathrm{v}}(s)$ and $G_{\mathrm{v\_dc}}(s)$ can be written as:

$$G_{\mathrm{v}}(s) = K_{\mathrm{p\_}v} + \frac{K_{\mathrm{i\_v}}}{s} \tag{32}$$

$$G_{\mathrm{v\_dc}}(s) = \frac{(U_{\mathrm{dc}}/i_{\mathrm{dc}})(1-d_{\mathrm{sc}})(1-\frac{L_{\mathrm{sc}}s}{(U_{\mathrm{dc}}/i_{\mathrm{dc}})(1-d_{\mathrm{sc}})^2})}{2 + (U_{\mathrm{dc}}/i_{\mathrm{dc}})C_{\mathrm{dc}}s} \tag{33}$$

From Eqs. (31), (32) and (33), open-loop transfer function of voltage control loop $G_{\mathrm{ol\_v}}(s)$ can be written as:

$$G_{\mathrm{ol\_v}}(s) = G_{\mathrm{v}}(s)G_{\mathrm{cl\_sc}}(s)G_{\mathrm{v\_dc}}(s) \tag{34}$$

Hence, Eq. (34) shows that the transfer function of the voltage control loop is totally independent of L_{g}.

Controllers are designed for high bandwidth and good stability margin by using diagram-aided method. K_{pwm} is assumed as unity. Figure 10 shows the open-loop Bode plots of voltage control loop, which is having good phase and gain margins of 76.6° and 10 dB, respectively. Now, phase margin and gain margin of the voltage control loop are totally independent of grid inductance. Therefore, the proposed voltage control scheme provides absolute stability and robustness under even very large values of grid inductance, whereas conventional voltage control loop provided stability only for the limited (max. 3 mH in this case) and small values of the grid inductance.

Open-loop Bode plots of the grid current control loop with different values of L_{g} are shown in Fig. 11. Large variations

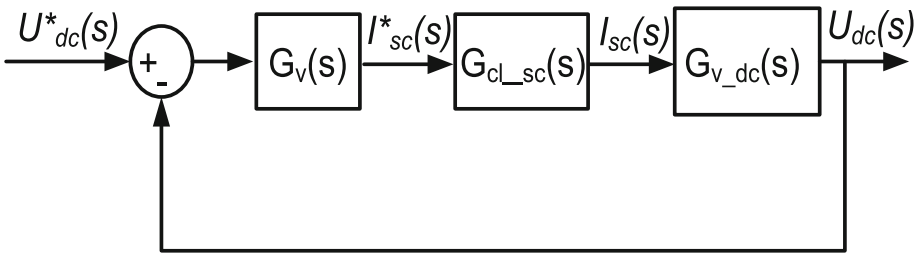

Fig. 9 Block diagram of voltage controller with proposed control scheme

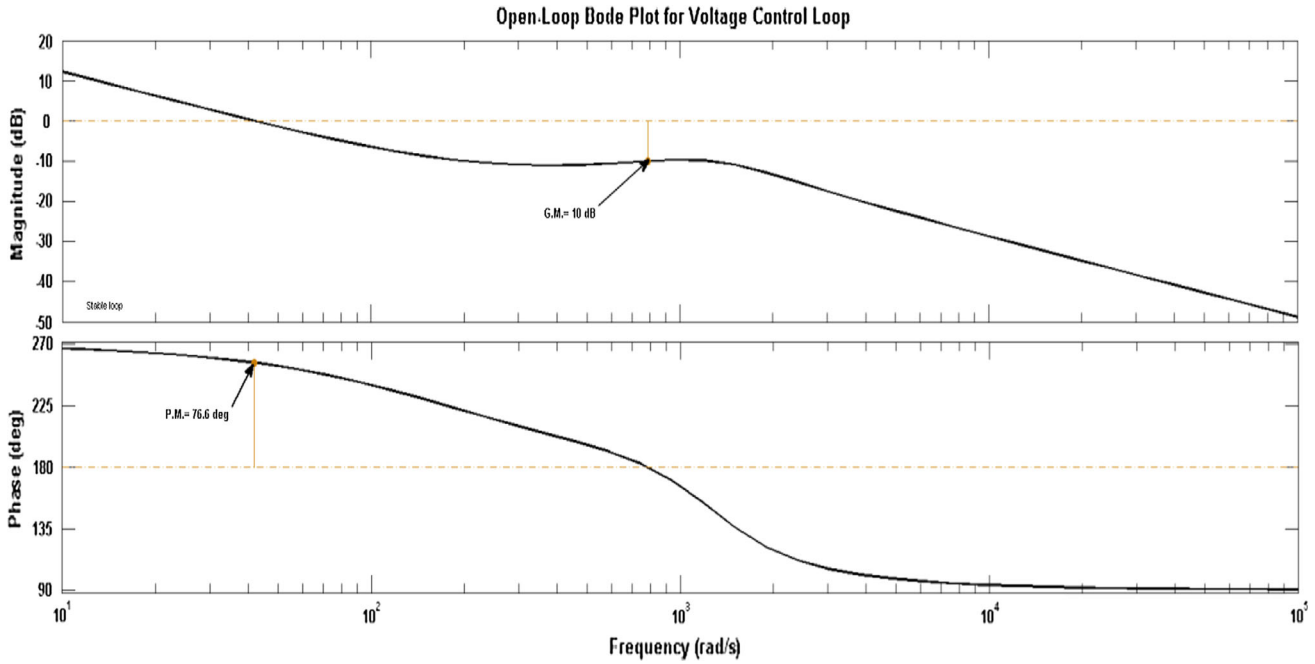

Fig. 10 Bode plots of the voltage control loop

in grid inductance are considered, ranging from $L_g = 0$ to 6 mH, to analyze the stability of the grid current control loop. Unlike the conventional control scheme, grid current control loop in proposed control scheme provides much better stability margins. In conventional control, system stability is limited up to $L_g = 3$ mH only whereas in the proposed control scheme, system stability margins with respect to grid inductance are increased significantly where stability being ensured even up to $L_g = 6$ mH. Therefore, although the grid current control loop is still dependent on grid inductance, but the stability margins provided are much better and up to large values of L_g.

3.3 Determination of the Stability Region

The impact of the grid inductance of the weak grid on the stability of the system is analyzed using the conventional and proposed control scheme. The grid inductance is the parameter of the system into Eqs. (25) and (31) which influence the behavior of the system. The analysis shown in this section to quantify the impact of the grid inductance on the stability of the system. Figures 12 and 13 plot the locus of the eigenvalues of the system under variation in the grid inductance. These plots are obtained by observing the movements of the eigenvalues of the weak grid-connected inverter model. The movements of the eigenvalues are obtained by incrementing the values of the grid inductance around 20 different operating values from 0 to 6 mH. As observed, this variation moves the eigenvalues of the system toward the imaginary axis causing slower response as discussed in result section and further closeness to instability.

Figure 12 shows the movements of the locus of the eigenvalues of the system with the conventional control scheme. The eigenvalues move closer toward the imaginary axis as grid inductance increases and also closes to the instability. The two conjugate eigenvalues cross the imaginary axis from negative real part to positive real part at the grid inductance of 3 mH. The system becomes unstable when the grid inductance value is more than 3 mH. Therefore, the stability region of the system with the conventional control scheme lies between the grid inductance value of 0–3 mH.

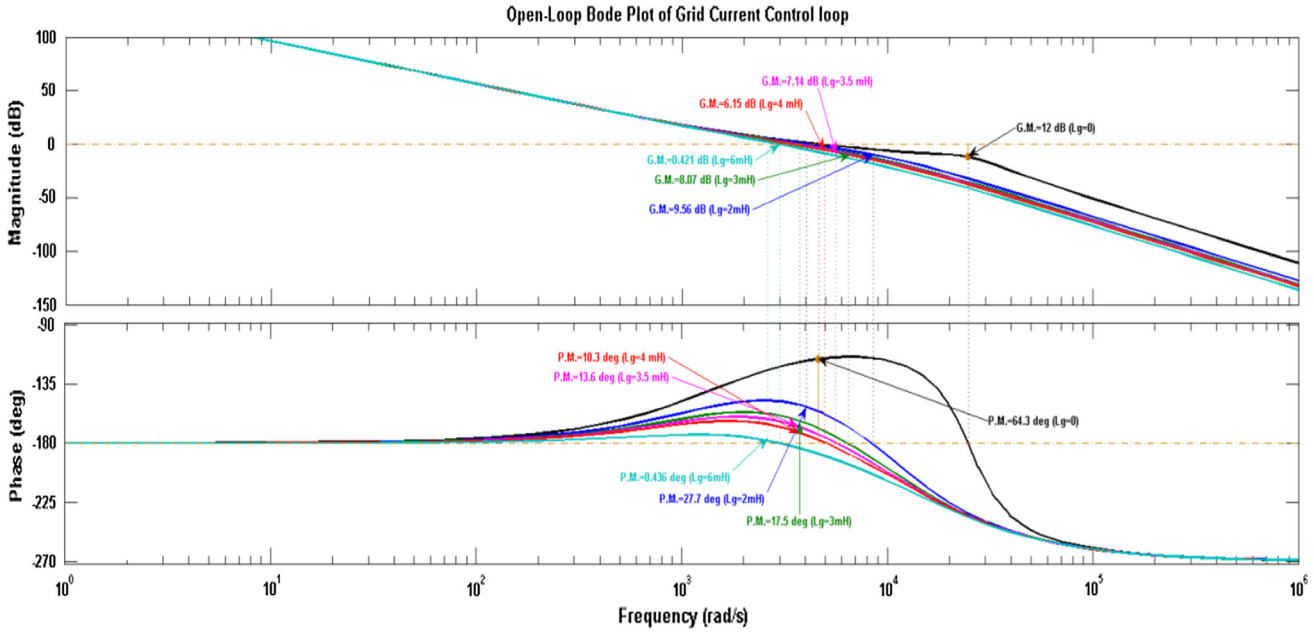

Fig. 11 Bode plots of the grid current control loop with different values of L_g

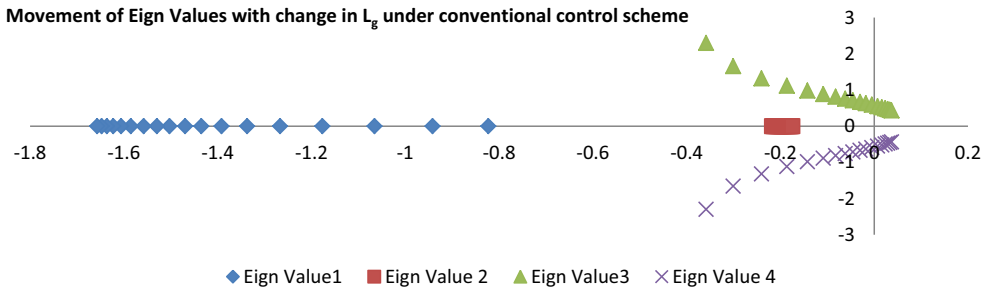

Fig. 12 Locus of the system eigenvalues with conventional control scheme under change in the grid inductance

Similarly, Fig. 13 reflects the movements of the eigenvalues of the system with the proposed control scheme. The two conjugate eigenvalues move toward the imaginary axis as grid inductance increases from 0 to 6 mH. But, in this case, eigenvalues cross the imaginary axis at 5.8 mH and instability arises. Therefore, the system stability region is from grid inductance value of 0–5.8 mH with the proposed control scheme. This analysis observes that the system stability region enhanced considerably with the proposed control scheme against the conventional control scheme. The approximately 90% increment of the stability bandwidth is achieved in this case with the proposed control scheme as compared to the conventional control scheme. Therefore, the proposed control scheme provides the improvement in the system stability as discussed and analyzed above in this section.

4 Results and Discussion

The proposed novel control strategy has been implemented in a 100-kW HES under the weak grid condition. To demonstrate the performance of the proposed control strategy, the system is simulated in MATLAB under different operating conditions. The system parameters, as used in simulation, are given in Tables 1 and 2.

Variable solar irradiance is chosen to study the system performance under different weather conditions, besides assessing the system performance under load changes. To establish the improved performance of the proposed control strategy, results are discussed and compared with that of conventional control strategy. Figure 14 shows the waveforms of varying irradiance as input to PV panel with change at 1 and 3 s to introduce the transient conditions in the system.

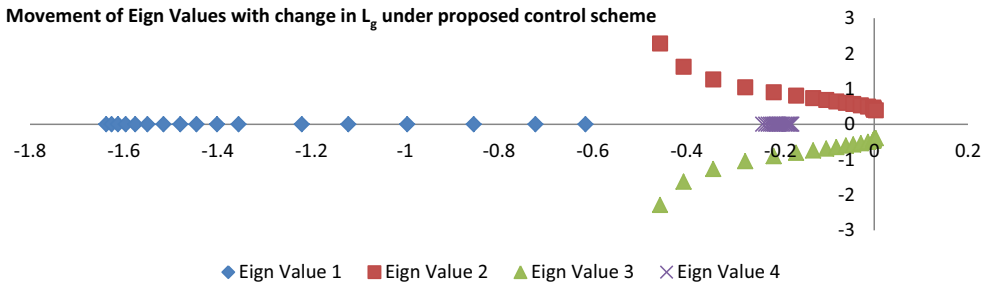

Fig. 13 Locus of the system eigenvalues with proposed control scheme under change in the grid inductance

Table 1 Storage device parameters

Super-capacitor	58 F, 16 V, 10 no. connected in series
L_{sc}	4 mH
v_{sc}	160 V
U_{dc} nominal	450 V
i_{dc} nominal	220 A
d_{sc} nominal	0.33

Table 2 Nominal system parameters

PV system rating	100 kW
Ac bus voltage rating, v_p	220 V
C_{pv}	100 uF
L_{pv}	3 mH
C_{dc}	1000 uF
L_1	0.36 mH
L_2	0.6 mH
C_f	7 uF

Figure 15 shows the waveforms of DC link voltage with proposed control scheme and the conventional control scheme. It is evident from Fig. 15 that under transient conditions, at the start time and at 1 s, the waveform of DC link voltage with proposed control indicates better transient response as compared to conventional control. It can be seen that under transient conditions, the DC link voltage shows large oscillations and slow response with conventional control, whereas with proposed control, the DC link voltage regulation is faster and waveform has relatively smaller oscillations and is smoother.

In Fig. 16, DC link voltage waveform is analyzed when irradiance is changed at 1 s. It can be clearly brought out that the dynamic response of voltage control loop with proposed control is better as it takes 0.3 s for DC link voltage to settle in comparison with conventional control, where its takes 0.5 s. Steady-state error due to harmonics is also minimized in proposed control scheme, whereas in conventional control, DC link voltage has steady-state error as seen in waveform after 1.5 s.

Figure 17 shows the DC link voltage waveform under varying grid inductance with a conventional control scheme to analyze the stability and robustness of the control scheme. As clearly shown in Fig. 15, the waveform gets adversely affected by an increase in grid inductance, so much so that it even goes unstable at 3 mH grid inductance.

On the other hand, the proposed control scheme provides better stability margin for voltage control loop under variable grid inductance as can be seen from Fig. 18. DC link voltage waveform is smooth and regulated under transient conditions with different grid inductance which establishes the improved performance of the proposed control scheme as well as better stability and robustness of the controller.

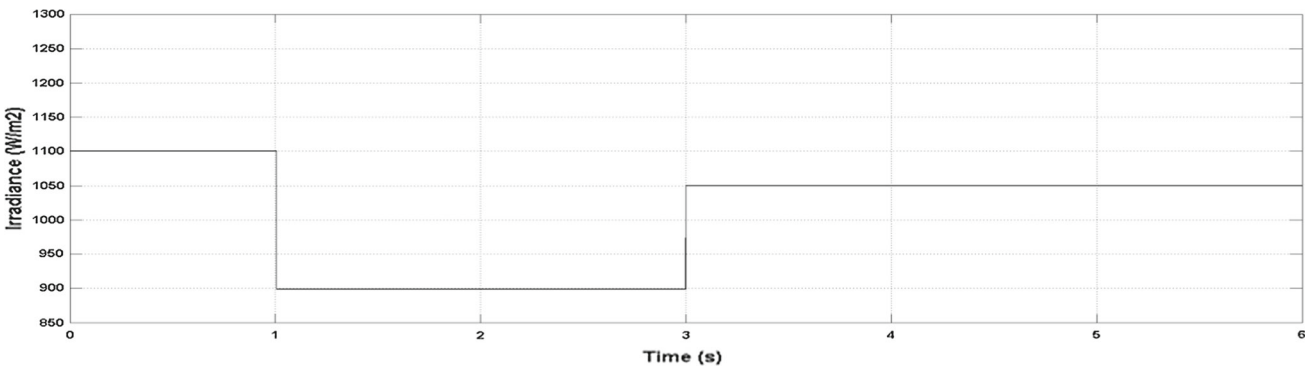

Fig. 14 Waveform of solar irradiance

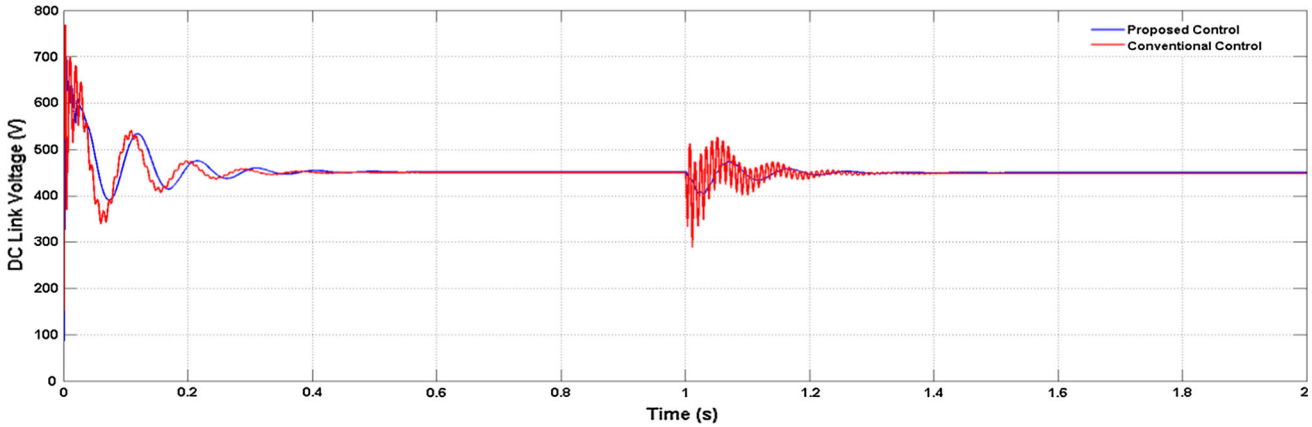

Fig. 15 Waveform of DC link voltage

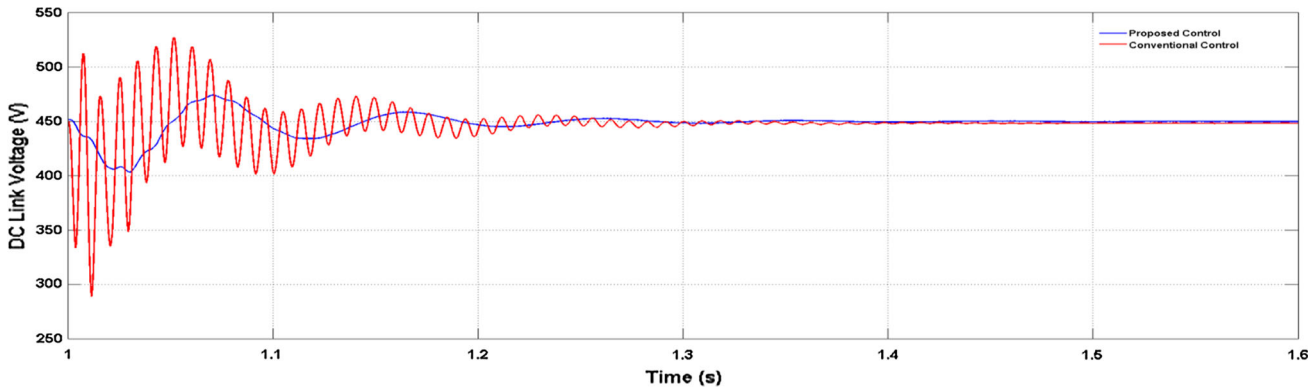

Fig. 16 Waveform of DC link voltage under change in irradiance

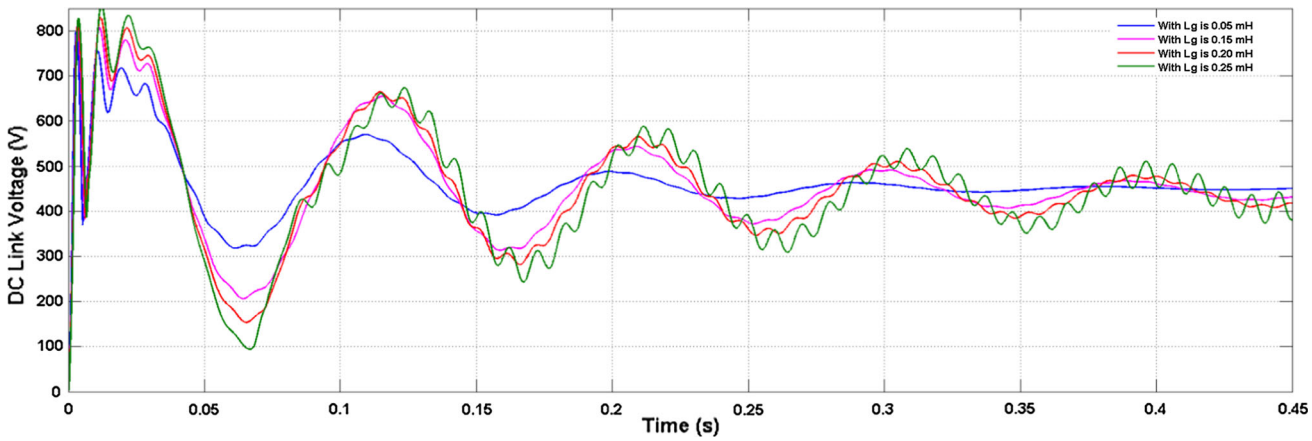

Fig. 17 DC link voltage under different grid inductance with conventional control scheme

Figure 19 shows the variations of d-axis grid current and SC current which clearly reflects that under transient conditions, initially SC current regulates the DC link voltage and balancing power and when grid current control loop is able to regulate the DC link voltage and power balancing, then SC current reduces.

In Fig. 20, three-phase grid voltage is shown with proposed and conventional control schemes, where under transient conditions at 1 s, the grid voltage is constant and the disturbance is negligible with the proposed control scheme, whereas with the conventional control scheme, grid voltage is distorted significantly and gets reestablished after long time.

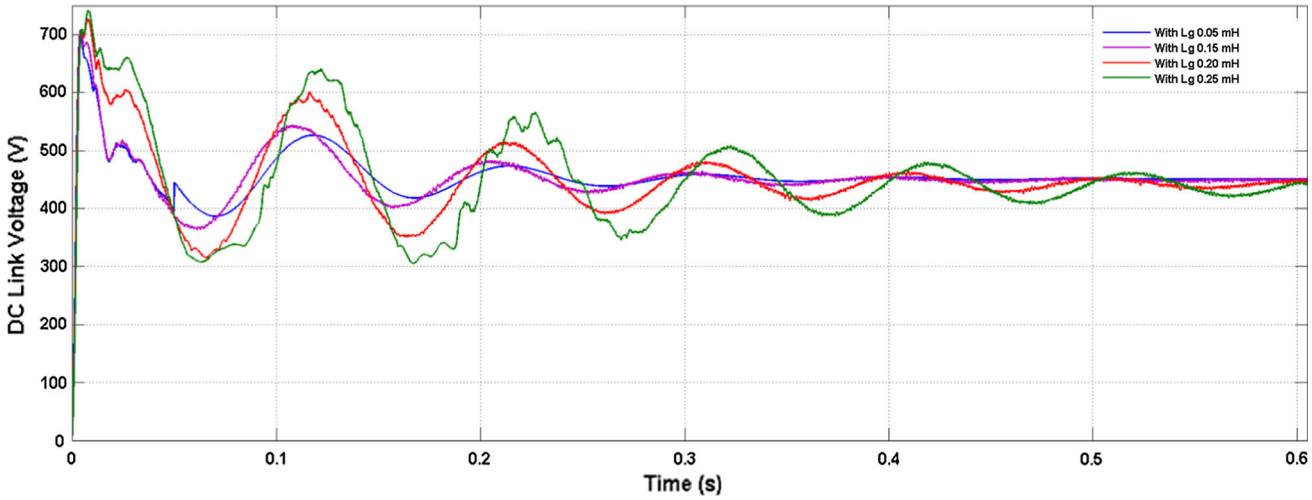

Fig. 18 DC link voltage under different grid inductance with proposed control scheme

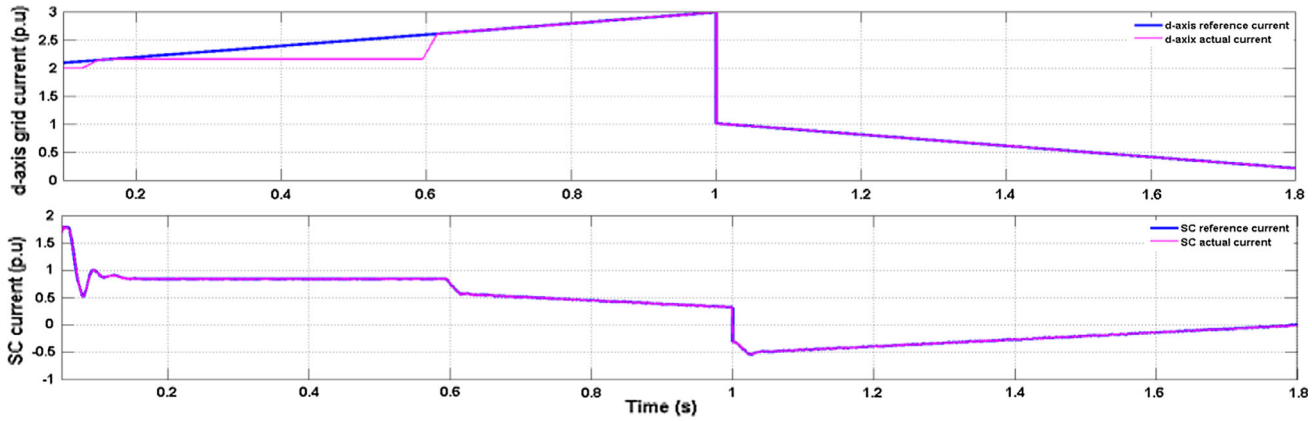

Fig. 19 d-axis grid current and SC current

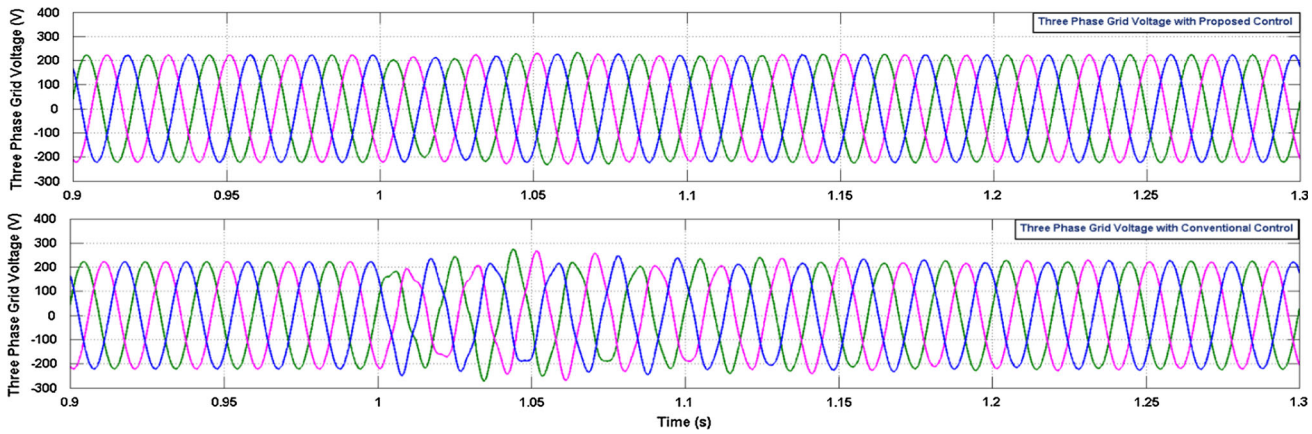

Fig. 20 Waveforms of three-phase grid voltage

Similarly, in Fig. 21, three-phase grid current waveforms with proposed and conventional control schemes are shown. Proposed control scheme improves the transient response of grid current and change in grid current is smooth under a change in operating conditions, but the same is not true with conventional control where the waveform of grid current is distorted.

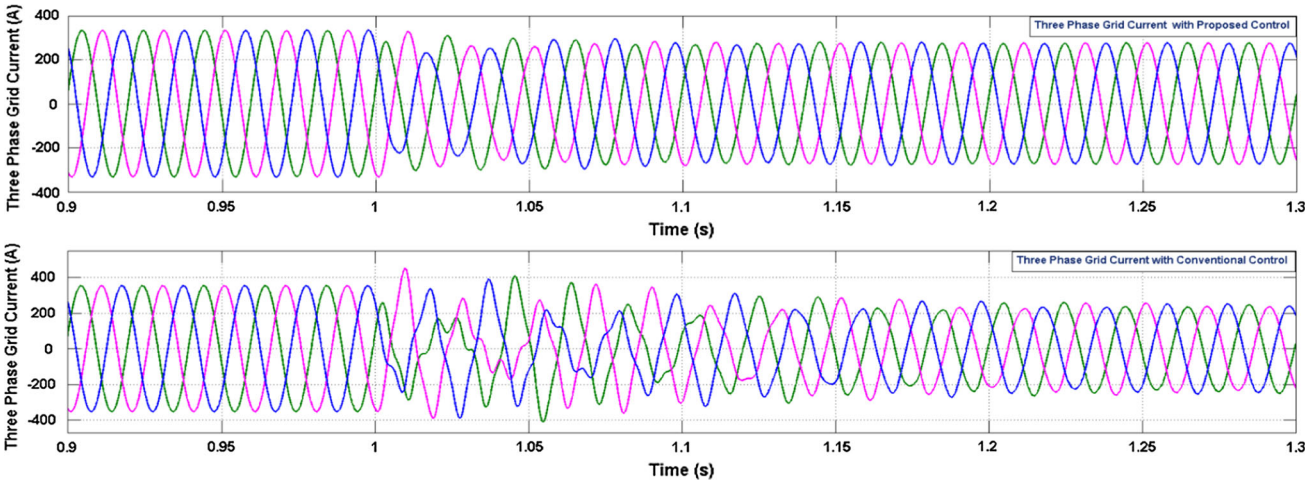

Fig. 21 Waveforms of three-phase grid currents

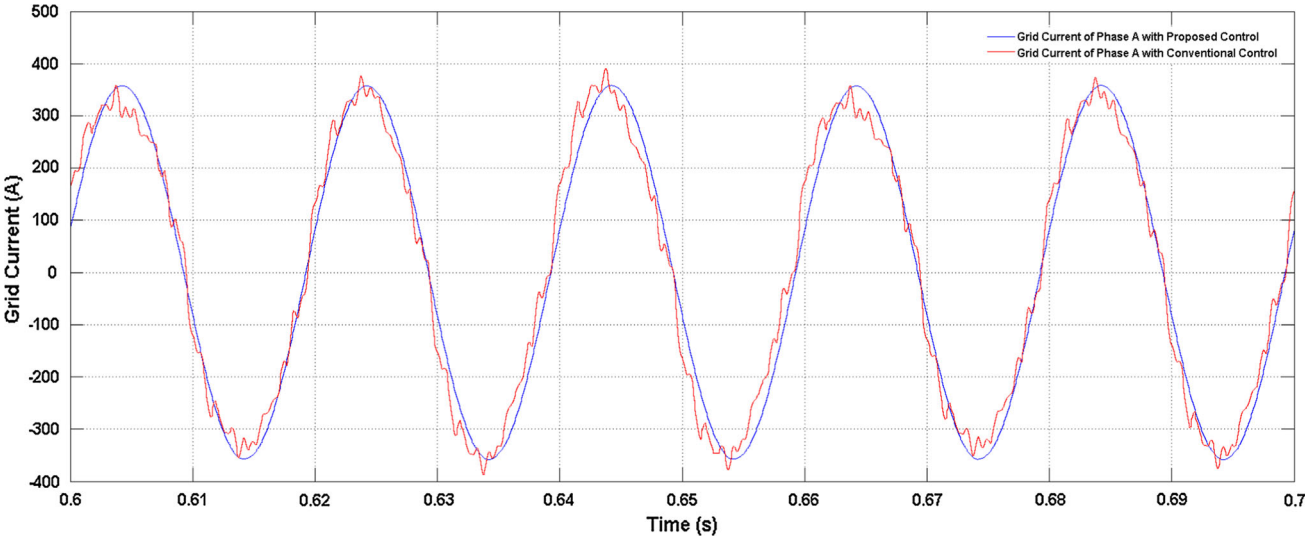

Fig. 22 Waveform of phase A grid current

Phase A grid current is shown in Fig. 22 with proposed and conventional control schemes, where the waveforms clearly indicate that the proposed control scheme is able to effectively suppress the ripples in the grid current while conventional control is not able to damp out the ripples in the grid current under the steady-state condition.

Figure 23 shows the effective control of reactive power regulation to improve power factor at PCC with the help of the proposed control scheme. Grid current reference for q-axis is chosen as zero to get unity power factor. It is visible in Fig. 23, through the waveforms of current and voltage of phase A, that the power factor of the system at PCC is unity.

The proposed control scheme is also implemented and validated under different operating conditions as shown in Fig. 24. DC link voltage waveforms have shown the effectiveness of the proposed control scheme under weak grid, stiff grid with transformer, islanded and overvoltage conditions. When the overvoltage condition occurs due to the lightly loaded grid condition, SC gets in charging mode (consumes power) to reduce the power injection into the grid and also to maintain DC link voltage constant. Reducing the power injected into the grid helps to lower down the voltage level within the limits while at the same time not having any adverse effect on the grid overvoltage condition. Not only this, as can be seen from Fig. 24, under operating conditions other than weak grid also, the proposed control scheme is very effective in regulating the DC link voltage.

Figure 25 shows the effectiveness of the proposed control scheme under grid unbalancing condition when grid voltage is unbalanced. The proposed control scheme is able to main-

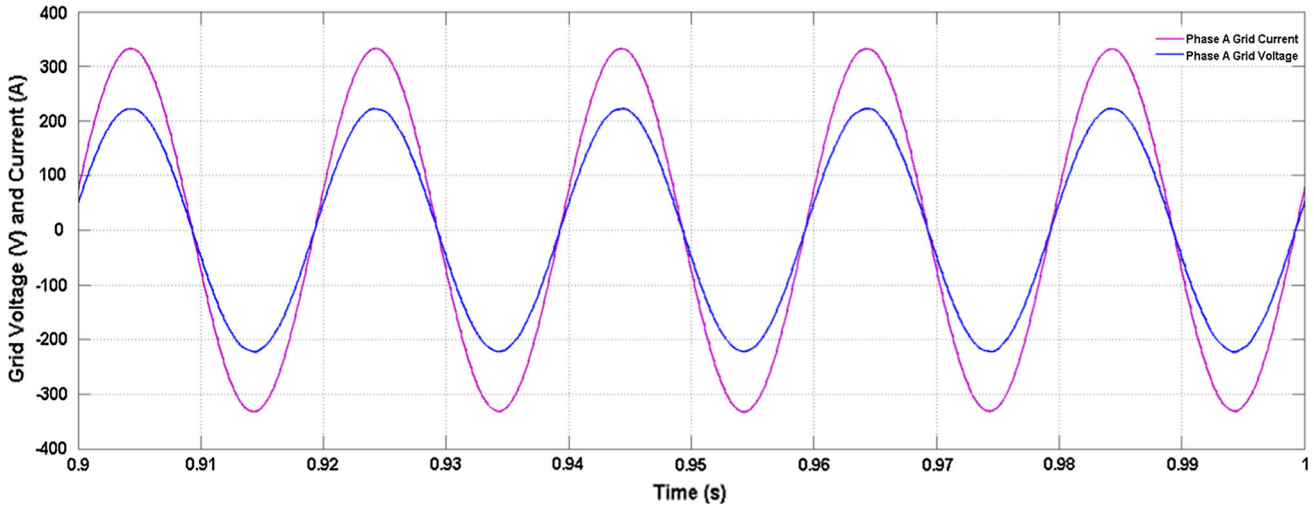

Fig. 23 Waveform of phase A grid current and voltage

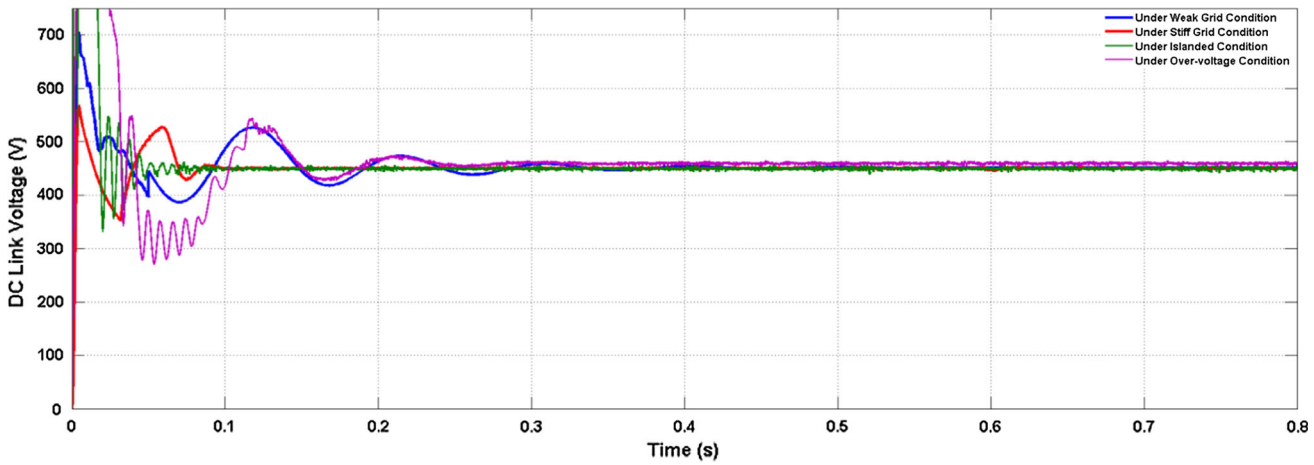

Fig. 24 Waveform of DC link voltage under different operating conditions

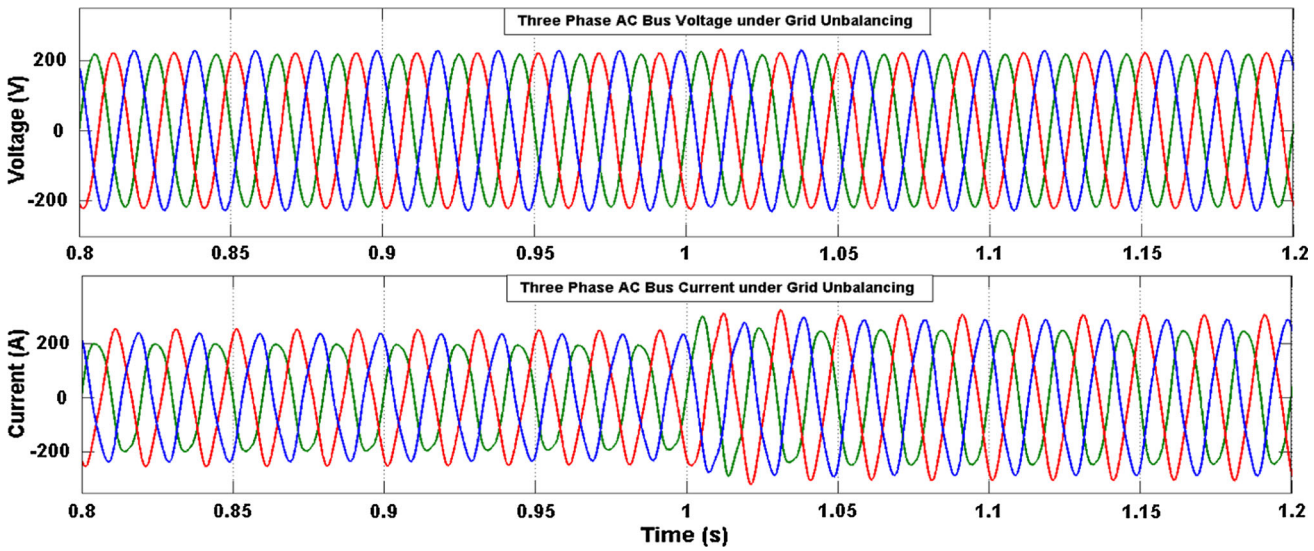

Fig. 25 Three-phase AC bus voltage and current under grid unbalance condition

tain the three-phase ac bus voltage balanced by regulating the three phase AC current. As clearly seen, in the figure that AC voltage is constant throughout the operating period as even under unbalanced and change in input irradiance conditions, but AC currents are different in phases to maintain the AC bus voltage.

5 Conclusions

The novel control strategy has been proposed to improve power quality with the help of SC for HES under weak grid condition. This paper has designed and analyzed the proposed control scheme to improve the dynamic response, stability margin and power quality of the HES under the weak grid condition. Results of HES have shown the improved and effective performance of the HES under transient as well as steady-state conditions in the weak grid environment. Comparative analysis of results with the conventional control scheme reveals that the transient and dynamic responses are improved considerably with the proposed control scheme. Stability and robustness of the voltage as well as grid current controllers are improved under the wide variations of the grid impedance in the weak grid. Not only the steady-state ripples in grid current are damped out, but the adverse effects of the coupling terms in grid current and voltage waveforms are also suppressed and hence, waveform quality is improved. Besides the weak grid condition, the proposed control scheme has also improved dynamic and steady-state response under other operating conditions such as stiff grid, islanding and overvoltage conditions. The result waveforms clearly indicate the power quality improvement with the proposed control strategy. The proposed control scheme is very effective in maintaining the AC bus voltage constant even under the grid unbalancing conditions. The proposed control scheme may be extended further to improve the power quality under islanding microgrid environment. Hardware implementation and analysis is the future scope of the study to evaluate more realistic performance of the proposed control scheme of the HES/alternate energy systems.

References

1. Sharma, R.; Sathans.: Survey on hybrid (wind/solar) renewable energy system and associated control issues. In: Proceedings of the IEEE 6th India International Conference on Power Electronics (IICPE), pp. 1-6 (2014)
2. Nehrir, M.H.; et al.: A review of hybrid renewable/alternative energy systems for electric power generation: configurations, control, and applications. IEEE Trans. Sustain. Energy **2**, 392–403 (2011)
3. Han, H.; Hou, X.; Yang, J.; Wu, J.; Su, M.; Guerrero, J.M.: Review of power sharing control strategies for islanding operation of AC microgrids. IEEE Trans. Smart Grid **7**, 200–215 (2016)
4. Mei, S.; Chen, L.: Recent advances on smart grid technology and renewable energy integration. Sci. China Technol. Sci. **52**, 3040–3048 (2013)
5. Tran, T.V.; Chun, T.W.; Lee, H.H.; Kim, H.G.; Nho, E.C.: PLL-based seamless transfer control between grid-connected and islanding modes in grid-connected inverters. IEEE Trans. Power Electron. **29**, 5218–5228 (2014)
6. Xu, J.; Xie, S.; Tang, T.: Improved control strategy with grid-voltage feedforward for LCL-filter-based inverter connected to weak grid. IET Power Electron. **7**, 2660–2671 (2014)
7. Ashabani, M.; Mohamed, Y.A.R.I.; Mirsalim, M.; Aghashabani, M.: Multivariable droop control of synchronous current converters in weak grids/microgrids with decoupled dq-axes currents. IEEE Trans. Smart Grid **6**, 1610–1620 (2015)
8. Tang, X.; Hu, X.; Li, N.; Deng, W.; Zhang, G.: A novel frequency and voltage control method for islanded microgrid based on multienergy storages. IEEE Trans. Smart Grid **7**, 410–419 (2016)
9. Xiao, H.; Luo, A.; Shuai, Z.; Jin, G.; Huang, Y.: An improved control method for multiple bidirectional power converters in hybrid AC/DC microgrid. IEEE Trans. Smart Grid **7**, 340–347 (2016)
10. Banerji, A.; Biswas, S.K.; Singh, B.: Enhancing quality of power to sensitive loads with microgrid. IEEE Trans. Ind. Appl. **52**, 360–368 (2016)
11. Zhang, P.; Zhao, H.; Cai, H.; Shi, J.; He, X.: Power decoupling strategy based on 'virtual negative resistor' for inverters in low-voltage microgrids. IET Power Electron **9**, 1037–1044 (2016)
12. Guan, Y.; Guerrero, J.M.; Zhao, X.; Vasquez, J.C.; Guo, X.: A new way of controlling parallel-connected inverters by using synchronous-reference-frame virtual impedance loop-part i: control principle. IEEE Trans. Power Electron. **31**, 4576–4593 (2016)
13. Wu, T.; Liu, Z.; Liu, J.; Wang, S.; You, Z.: A unified virtual power decoupling method for droop-controlled parallel inverters in microgrids. IEEE Trans. Power Electron. **31**, 5587–5603 (2016)
14. Li, C.; Chaudhary, S.K.; Savaghebi, M.; Vasquez, J.C.; Guerrero, J.M.: Power flow analysis for low-voltage AC and DC microgrids considering droop control and virtual impedance. IEEE Trans. Smart Grid **10**, 1109 (2016)
15. Baharizadeh, M.; Karshenas, H.R.; Guerrero, J.M.: Control strategy of interlinking converters as the key segment of hybrid AC–DC microgrids. IET Gener. Transm. Distrib. **10**, 1671–1681 (2016)
16. Gee, A.M.; Robinson, F.V.P.; Dunn, R.W.: Analysis of battery lifetime extension in a small-scale wind-energy system using supercapacitors. IEEE Trans. Energy Convers. **28**, 24–33 (2013)
17. Baronti, F.; Fantechi, G.; Roncella, R.; Saletti, R.: High-efficiency digitally controlled charge equalizer for series-connected cells based on switching converter and super-capacitor. IEEE Trans. Ind. Inform. **9**, 1139–1147 (2013)
18. Reznik, A.; Simões, G.M.; Al-Durra, A.; Muyeen, S.M.: LCL filter design and performance analysis for grid-interconnected systems. IEEE Trans. Ind. Appl. **50**, 1225–1232 (2014)
19. Liserre, M.; Blaabjerg, F.; Hansen, S.: Design and control of an LCL-filter-based three-phase active rectifier. IEEE Trans. Ind. Appl. **41**, 1281–1291 (2005)
20. Leva, S.; Morando, A.P.: Analysis of physically symmetrical lossy three-phase transmission lines in terms of space vectors. IEEE Trans. Power Deliv. **21**, 873–882 (2006)
21. Xu, J.; Xie, S.; Tang, T.: Evaluations of current control in weak grid case for grid-connected LCL-filtered inverter. IET Power Electron. **6**, 227–234 (2013)
22. Kollimalla, S.K.; Mishra, M.K.; Narasamma, N.L.: Design and analysis of novel control strategy for battery and supercapacitor storage system. IEEE Trans. Sustain. Energy **5**, 1137–1147 (2014)

23. Dannehl, J.; Fuchs, F.W.; Hansen, S.; et al.: Investigation of active damping approaches for PI-based current control of grid-connected pulse width modulation converters with LCL filters. IEEE. Trans. Ind. Appl. **46**, 1509–1517 (2010)
24. Sun, J.: Impedance-based stability criterion for grid-connected inverters. IEEE Trans. Power Electron. **26**, 3075–3078 (2011)
25. Jin, Y.; Xu, J.; Zhou, G.; Mi C.: Small-signal modeling and analysis of improved digital peak current control of boost converter. In: Proceedings of the IEEE 6th International Power Electronics Motion Control Conference, pp. 326–330 (2009)